Chapter 5: EQUATION OF STATE

In Chapter 3, we assumed the approximated functions under a fixed volume per particle that predict the interaction energy and the interaction entropy of the cluster phase and the monomer phase, and confirmed the approximated functions well reproduce the MC results of the Helmholtz free energy of the homogeneous nucleation. In this chapter, we purpose to develop the equation of state (EOS) of Helmholtz free energy of the nucleation as a function of the number of particles N, temperature T, and volume per particle V/N by taking into consideration the dependence on the volume per particle of the thermodynamic properties. Moreover, we rearrange the EOS to estimate Gibbs free energy of the nucleation as a function of N, T, and pressure P by taking into consideration contributions of the pressure and the ideal gas term.

5.1. Volume Dependence of the Thermodynamic Properties

5.1.1. Monomer phase

As we stated above, interaction energy and interaction entropy of the monomer phase is assumed that it have no dependence on temperature. Before the discussion about the volume dependence of the thermodynamic properties, we consider whether the pressure of the monomer phase has the temperature dependence or not. Figure 5.1 shows the temperature dependence of the interaction term of pressure, $P^e = P - NkT/V$, in the phase transition calculation. Since the interaction pressure levels off against the temperature after the decomposition of the cluster, we assume the equilibrated value of the decomposed monomer phase in the phase transition calculation into the P^e of the monomer phase.

Here, the density dependence of the thermodynamic properties is discussed. On the assumption of the uniform distribution of particles of the monomer phase, the interaction energy can be expressed as

$$\frac{U_m^e}{N} = 4\pi\rho\int\phi(r)r^2dr, \tag{5.1}$$

where $\rho = N/V$ is the number density of the system. Accordingly, the interaction energy is predicted as in proportion to the system density, as

$$U_m{}^e/\rho = \text{const.} \tag{5.2}$$

Such behavior of the interaction energy of the monomer phase is shown in Fig. 5.2. In the figure (b), it is realized that the products of the $U_m{}^e$ and the volume per particle agree each other and the products can be approximated as a function of the number of particles. Secondly, the ideal gas equation of state obtains the entropy change of isothermal expansion ΔS_{exp} from the volume V_0 to V as

$$\Delta S_{\text{exp}} = Nk\ln(V/V_0). \tag{5.3}$$

Here, when we set a standard value $V_0/N = 1.0\ \sigma^3$, the expansion entropy is expressed as

$$\Delta S_{\text{exp}} = Nk\ln(V/N\sigma^3); \tag{5.4}$$

then the interaction entropy of the monomer phase is predicted as a function of N and V/N,

$$S_m^e(N, V/N) = S_m^e(N, V_0/N) + Nk\ln(V/N\sigma^3). \tag{5.5}$$

Figure 5.3 shows the behavior of the interaction entropy. The figure (b) shows the values that result when $k\ln(V/N\sigma^3)$ is subtracted from the interaction entropy per particle of the monomer phase for each density. Lastly, we consider the van der Waals equation to predict the V/N dependence of pressure of the monomer phase. That is,

$$P = \frac{NkT}{V - Nb} - a\rho^2, \tag{5.6}$$

where a and b are the van der Waals coefficients. The first term indicates the ideal gas term and a repulsive part of the interaction term, while the second term indicates an attractive part. In the monomer phase, the interaction almost occupied by the attractive part because the particles are scattered in the system and scarcely connected each other. That is to say, the interaction term of the pressure to be predicted as in proportion to the square of ρ, as $P_m{}^e/\rho^2 = \text{const.}$ The product of the interaction pressure of the monomer phase and the square of the volume per particle is plotted in Fig. 5.4.

On the basis of the above considerations and the approximated functions designed under a fixed volume per particle as eqs. 3.1 and 3.2, we defined approximated functions for the interaction energy, the interaction entropy, and the interaction term of pressure of the monomer phase that depend on the number of particles and the volume per particle as:[13,14]

$$\frac{U_m^e}{N} = \left\{ \sum_{i=0}^{2} a_i N^{-i} \right\} / (V/N), \tag{5.7}$$

$$\frac{S_m^e}{N} = \left\{ \sum_{i=0}^{2} b_i N^{-i} \right\} + k \ln(V/N), \tag{5.8}$$

$$\frac{P_m^e V}{N} = \left\{ \sum_{i=0}^{2} c_i N^{-i} \right\} / (V/N). \tag{5.9}$$

The pressure term is treated as $P_m{}^e V$ term per particle coordinate with the interaction energy and the interaction entropy. The coefficients a_i, b_i, and c_i are obtained by least-squares fittings similarly to Chapter 3, which results are shown in Table 3 and the fitted curves in Figs. 5.2-5.4. The relative deviations, that expressed like as eq. 3.5, $\delta'(U_m{}^e/N) = 0.0169$, $\delta'(S_m{}^e/N) = 0.0304$, and $\delta'(P_m{}^e V/N) = 0.00822$. Incidentally, the relative deviations of the interaction terms of the Helmholtz and the Gibbs free energies of the monomer phase are $\delta'(A_m{}^e/N) = 0.0299$ and $\delta'(G_m{}^e/N) = 0.0297$.

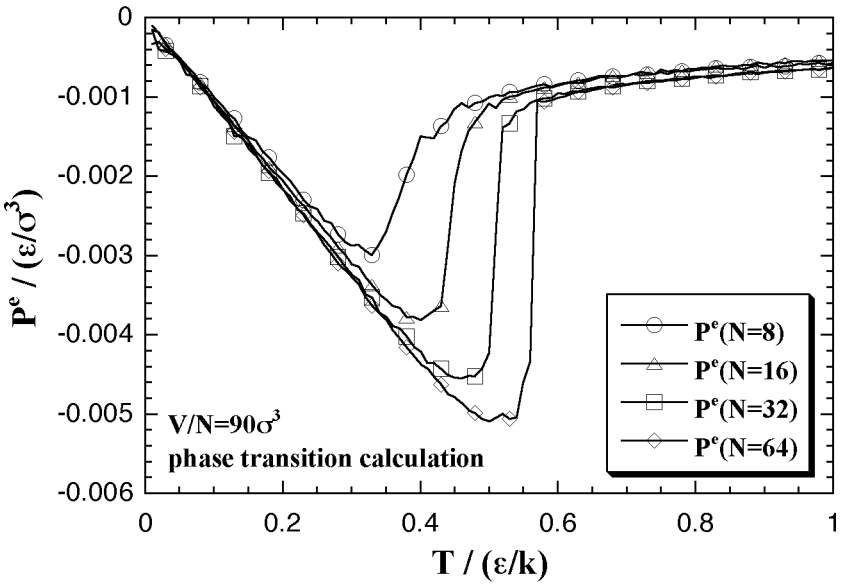

Fig. 5.1. Temperature dependence of the interaction term of pressure in the phase transition calculation at $V/N = 90\ \sigma^3$. The curves leveled off after decomposition of the cluster.

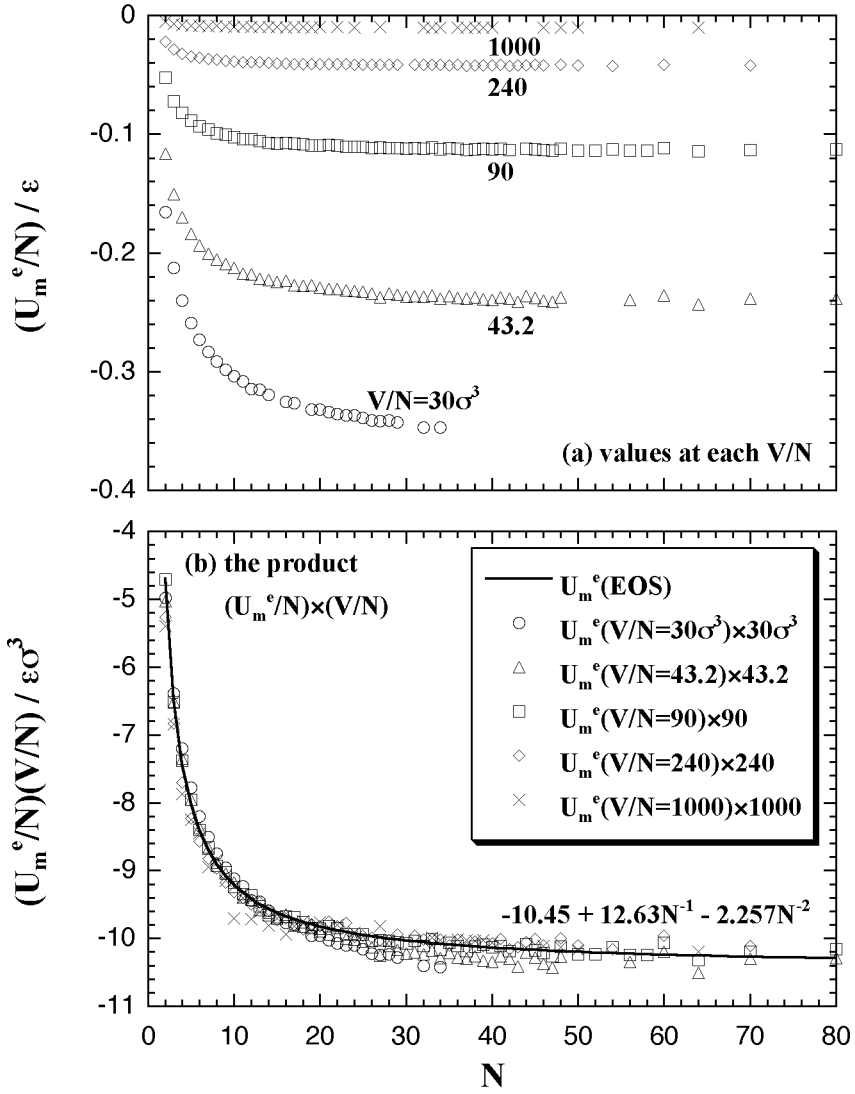

Fig. 5.2. Interaction energy of the monomer phase versus the number of particles plots on each volume per particle. The figure (a) shows the values at each simulated volume per particle, and (b) the product of the interaction energy and the volume per particle. The circles, triangles, squares, diamonds, and crosses show the MC result. The solid curve shows the result of the least-squares fitting by eq. 5.7.

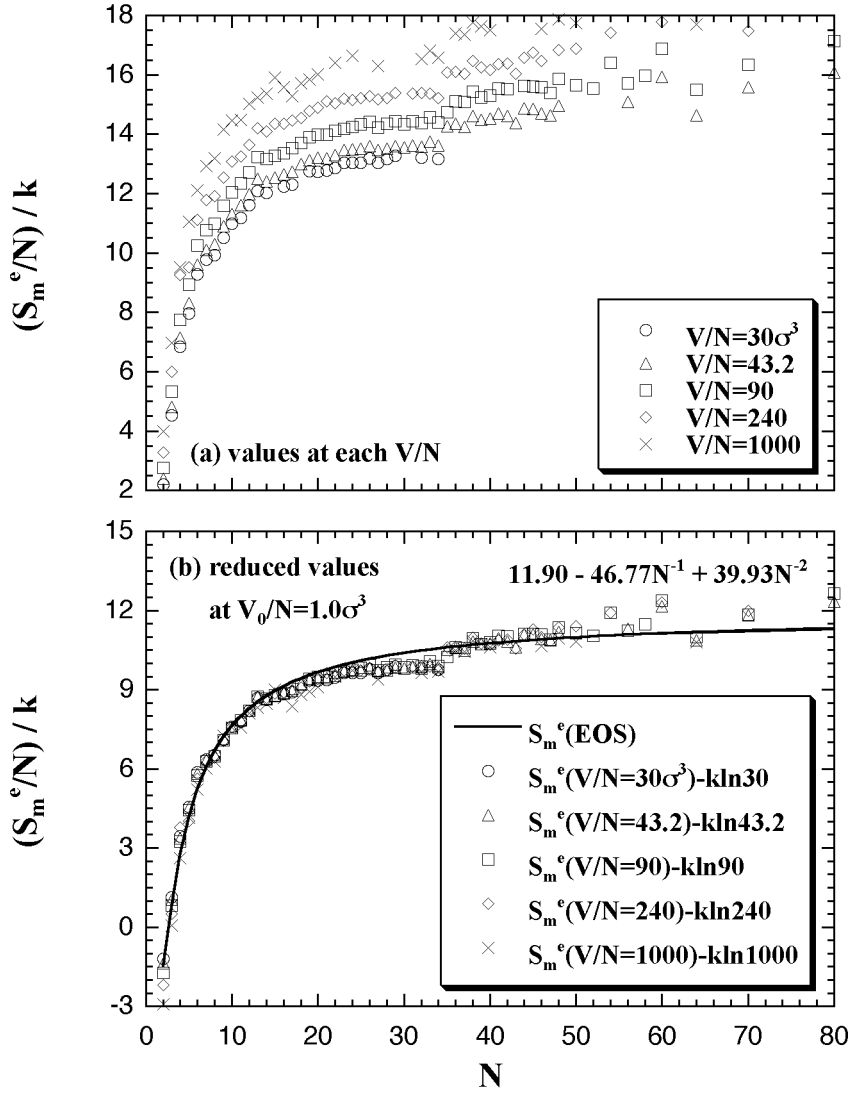

Fig. 5.3. The density dependence of the interaction entropy per particle of the monomer phase. The figure (a) shows the values at each simulated volume per particle, and (b) the reduced value into the standard of $V_0/N = 1.0\ \sigma^3$. The solid curve shows the result of the least-squares fitting by eq. 5.8.

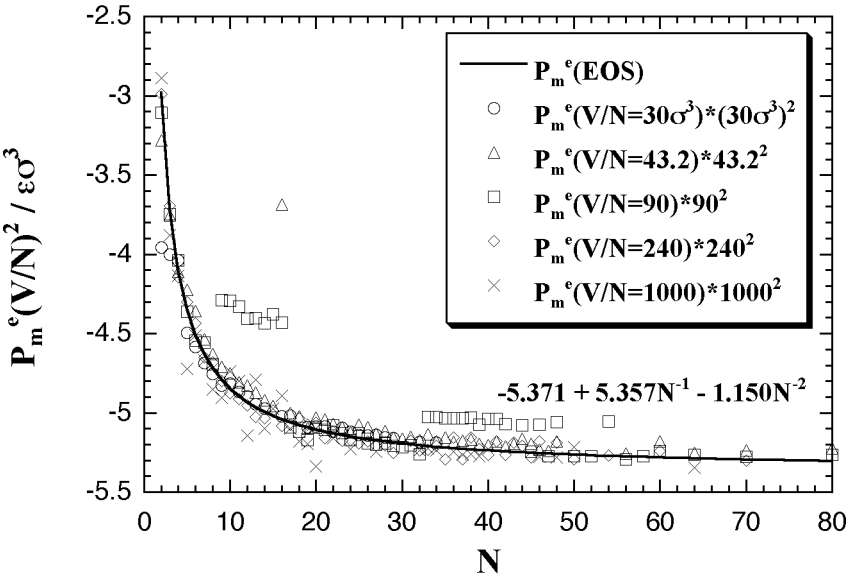

Fig. 5.4. The product of P_m^e and $(V/N)^2$ versus N plots. Similarly to the interaction energy and the interaction entropy, the products of the interaction pressures and the square of the volumes per particles roughly agree each other. The solid curve shows the result of the least-squares fitting by eq. 5.9.

Table 3. Results of the least-squares fittings for the monomer phase: a_i, b_i, and c_i.

i	a_i	b_i	c_i
0	−1.045E+1	1.190E+1	−5.371E+0
1	1.263E+1	−4.677E+1	5.357E+0
2	−2.257E+0	3.993E+1	−1.150E+0

Table 4. Results of the least-squares fittings for the cluster phase: a_{mn} and b_{pq}.

a_{mn}		m					
		2	1	0	−1	−2	−3
n	4	3.125E−2	−3.424E+0	1.222E+2	−1.027E+3	2.937E+3	−2.713E+3
	3	−6.758E−2	7.527E+0	−2.735E+2	2.417E+3	−7.041E+3	6.540E+3
	2	4.536E−2	−5.156E+0	1.899E+2	−1.831E+3	5.491E+3	−5.142E+3
	1	−9.449E−3	1.100E+0	−3.813E+1	4.436E+2	−1.400E+3	1.325E+3
	0	4.015E−4	−4.656E−2	3.000E+0	−2.137E+1	5.442E+1	−4.490E+1
	−1	8.790E−5	−2.183E−2	−4.362E+0	2.075E+1	−4.375E+1	3.581E+1

b_{pq}		p			
		0	−1	−2	−3
q	5	−5.208E+0	1.023E+2	−3.426E+2	3.161E+2
	4	1.332E+1	−3.012E+2	1.106E+3	−1.106E+3
	3	−1.080E+1	2.958E+2	−1.191E+3	1.269E+3
	2	3.496E+0	−1.059E+2	4.739E+2	−5.364E+2
	1	−1.425E+0	1.421E+1	−6.355E+1	7.562E+1
	0	9.166E−3	−3.736E−1	1.869E+0	−2.337E+0

5.1.2. Cluster phase

The density dependence of interaction energy, interaction entropy and interaction part of pressure term of the cluster phase is mentioned below. In our model, the cluster phase contains an N-particle cluster and no vapor phase particles in surroundings of the cluster, like Fig. 2.2. Since the model has no interaction between the cluster and the surroundings, if the shape of cluster was similar each other, there is no dependence on the system density in which thermodynamic properties. Such example is shown in Fig. 5.5 in the case of 27-particle systems; all the superheated clusters on each volume per particle are spherical similarly. On the contrary, the stretched cluster mentioned above, like as Fig. 4.2, disagrees with the spherical cluster in which thermodynamic properties. Such examples are shown in Fig. 5.6 in the case of 47-particle systems: the stretched cluster is obtained at $V/N = 90\ \sigma^3$. In the figures (a) and (b), the thermodynamic properties have disagreements each other at high-temperature (ca. $T > 0.7\ \varepsilon/k$). However, in the figure (c), the Helmholtz and the Gibbs free energies agree closely. The agreement is caused that the disagreements of U_c^e and S_c^e are canceled in the Helmholtz free energy and the disagreement of $P_c^e V$ term is much smaller ($10^{-2}\ \varepsilon$ order) than the values of the free energies.

In Chapter 3, we were obliged to approximate the interaction energy and the interaction entropy of the cluster phase separately. The dispersion of the interaction energy that was due to appearance of the stretched cluster caused the approximation by one function to be unsuccessful. Besides, in the aims of estimating the Helmholtz and Gibbs free energies, both the spherical cluster and the stretched cluster give roughly similar values. Accordingly, we removed the stretched clusters from the subjects of the approximation and attempted to approximate the interaction energy and the interaction entropy as one function. Figure 5.7 shows the states in which obtained the stretched clusters. The approximated functions for the U_c^e (and it also predicts the S_c^e) and the $P_c^e V$ term of the cluster phase are:

$$\frac{U_c^e}{NT} = \sum_m \sum_n \left\{ a_{mn} N^m T^n \right\}, \qquad (5.10)$$

$$(m = -3, -2, -1, 0, 1, 2;\ n = -1, 0, 1, 2, 3, 4)$$

$$\frac{P_c^e V}{N} = \sum_p \sum_q \left\{ b_{pq} N^p T^q \right\}. \qquad (5.11)$$

$$(p = -3, -2, -1, 0;\ q = 0, 1, 2, 3, 4$$

The approximation of eq. 5.10 is performed as (U_c^e/NT) for the purpose of fitting accuracy,

similarly to eq. 3.3. As results of the least squares fittings, we obtained the coefficients a_{mn} and b_{pq} as shown in Table 4 and the fitted curves as shown in Figs. 5.8 and 5.9. The relative deviations are $\delta'(U_c^e/NT) = 0.0190$ and $\delta'(P_c^eV/N) = 0.0327$. Incidentally, the relative deviations of the interaction entropy, the interaction terms of Helmholtz and Gibbs free energies of the cluster phase are $\delta'(S_c^e/T) = 0.0547$, $\delta'(A_c^e/T) = 0.0357$, and $\delta'(G_c^e/N) = 0.0343$.

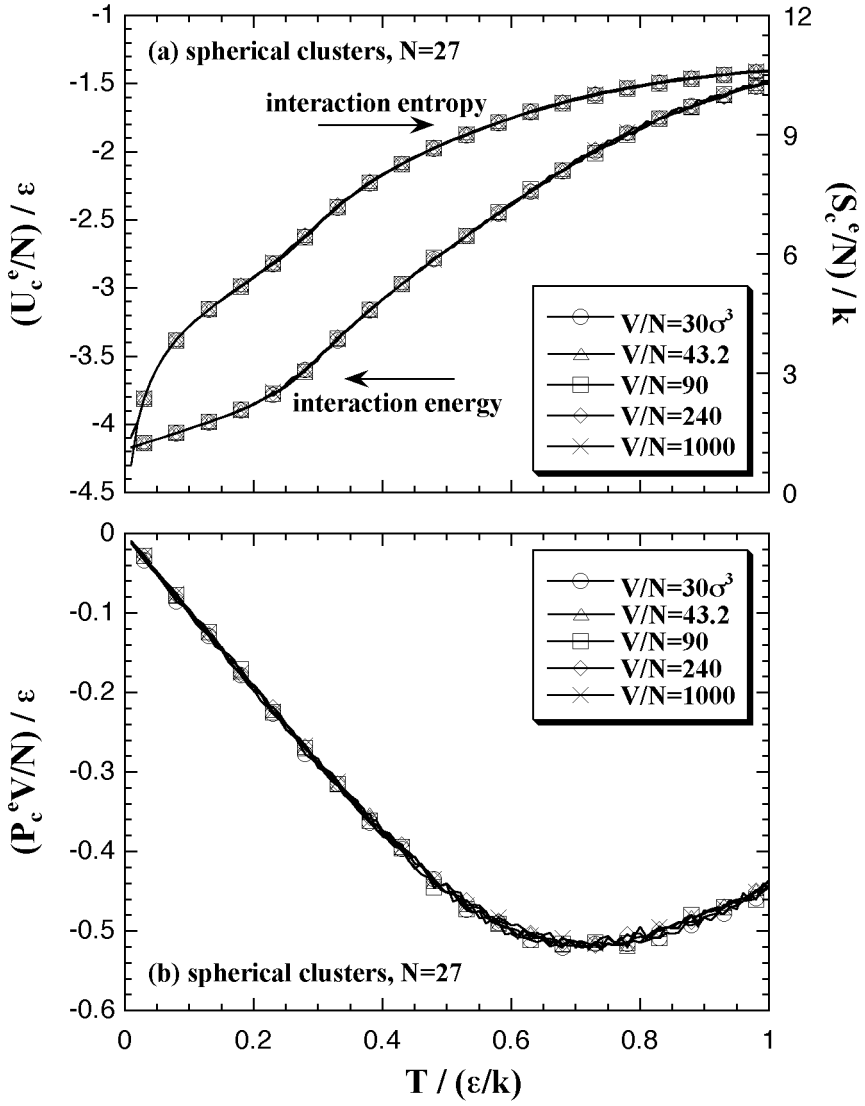

Fig. 5.5. The interaction energy, the interaction entropy, and the pressure term of the cluster phase calculations on each volume per particle in 27-particle system. The 27-particle systems obtain similarly spherical cluster phases on the each volume per particle.

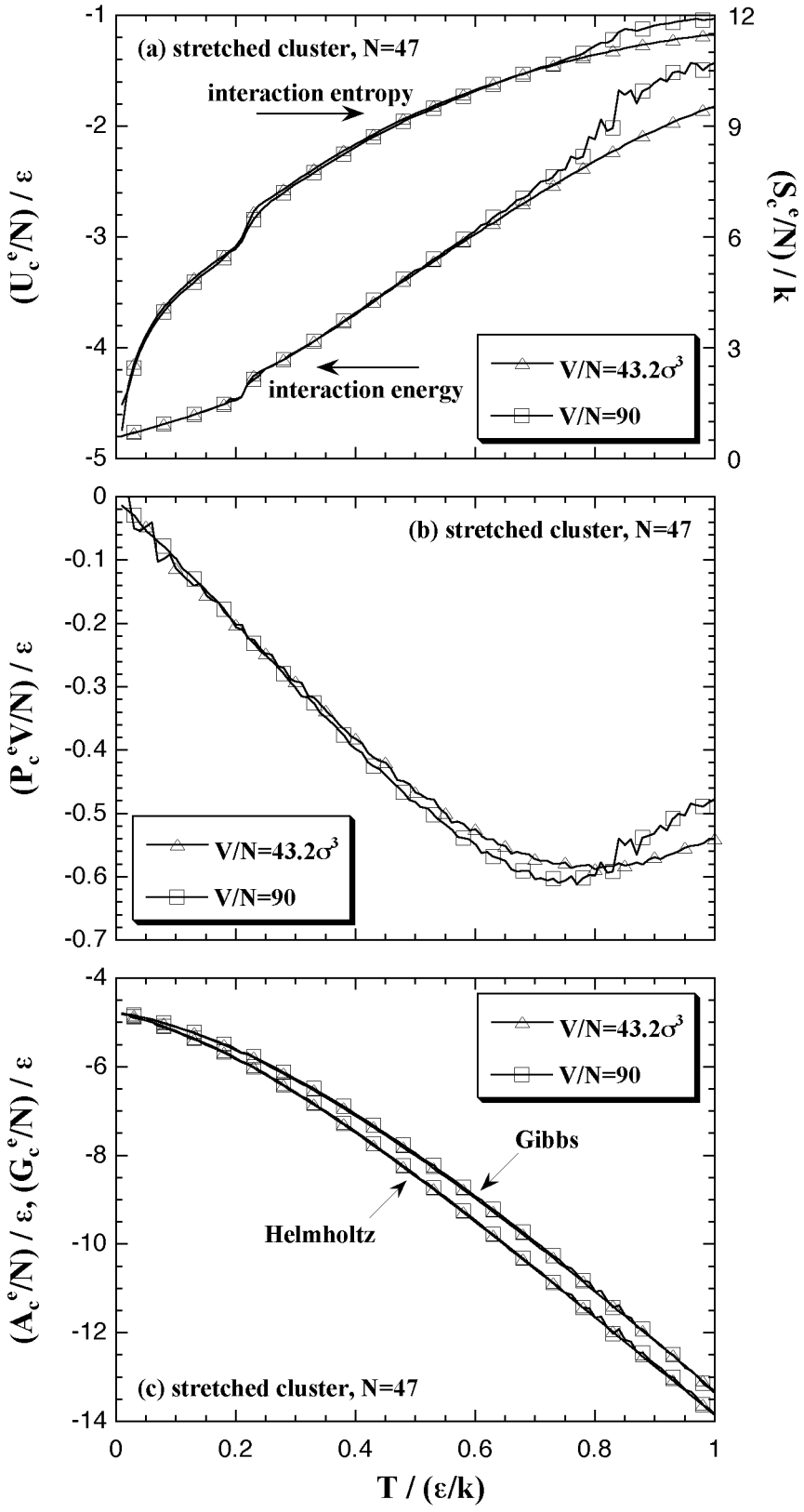

Fig. 5.6. The *V*/*N* dependence of the thermodynamic properties in 47-particle system. Though the U_c^e, S_c^e, and P_c^eV disagree on each volume per particle caused by the stretched cluster, there are no disagreements on the A_c^e and G_c^e.

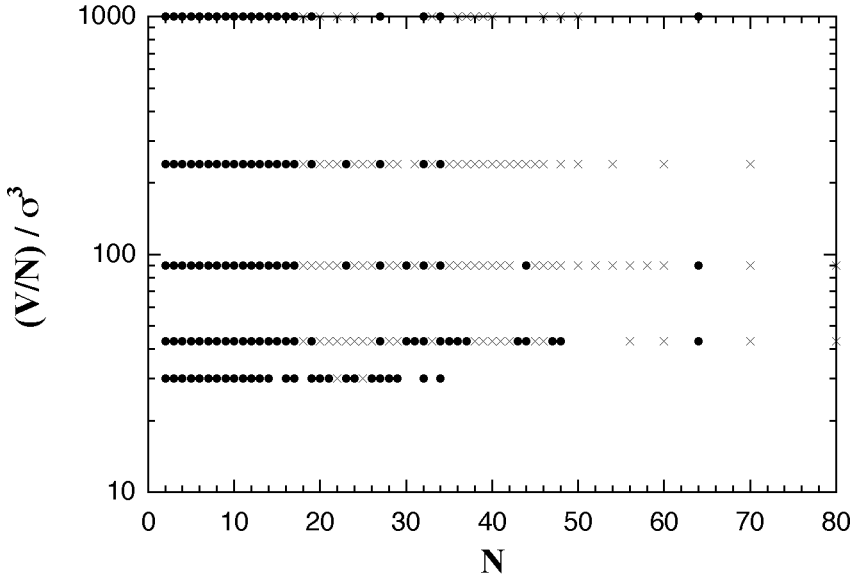

Fig. 5.7. Map of the states that are removed from the subjects of the cluster phase approximation. All the plots correspond to the simulated states as shown in Fig. 4.1, and the crosses are the states in which obtained the stretched clusters.

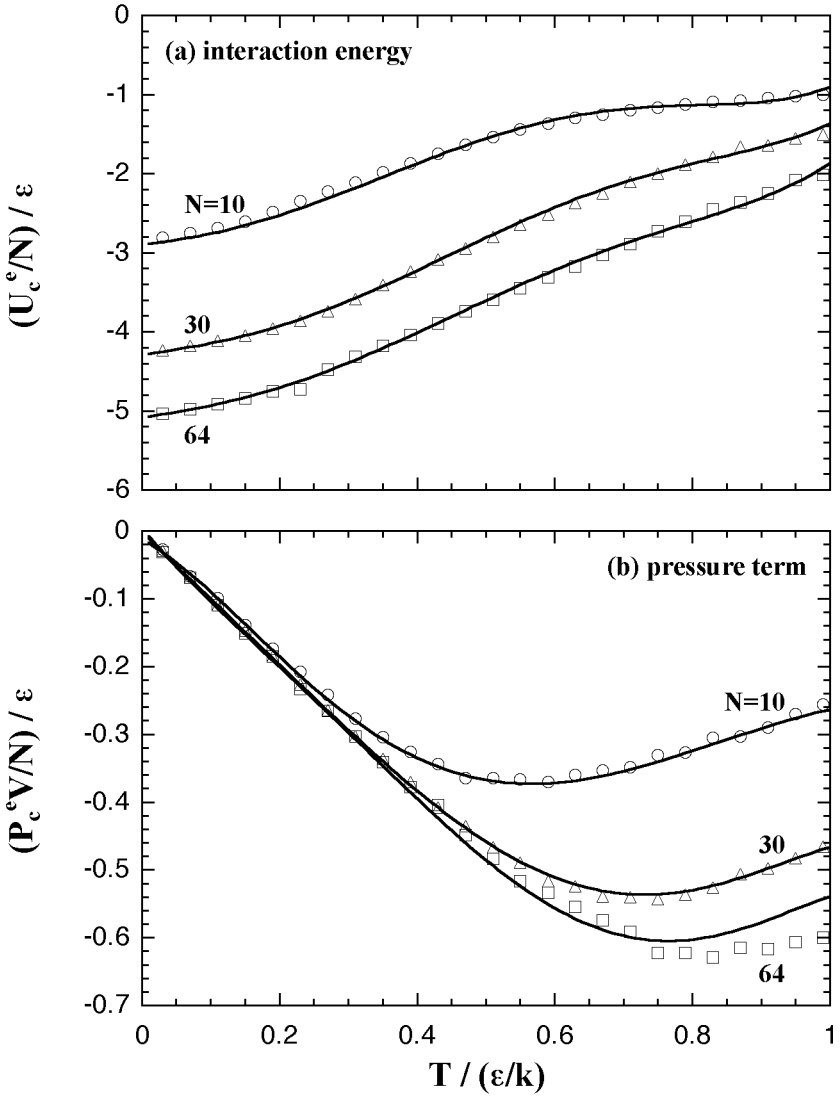

Fig. 5.8. Fitting results of the cluster phase: (a) the interaction energy, while (b) the product of the interaction term of pressure and volume per particle. The circles, triangles, and squares are the MC results and the curves are the EOS. Care should be taken that the approximated functions for the cluster phase, eqs. 5.10 and 5.11, have no dependence on the volume per particle.

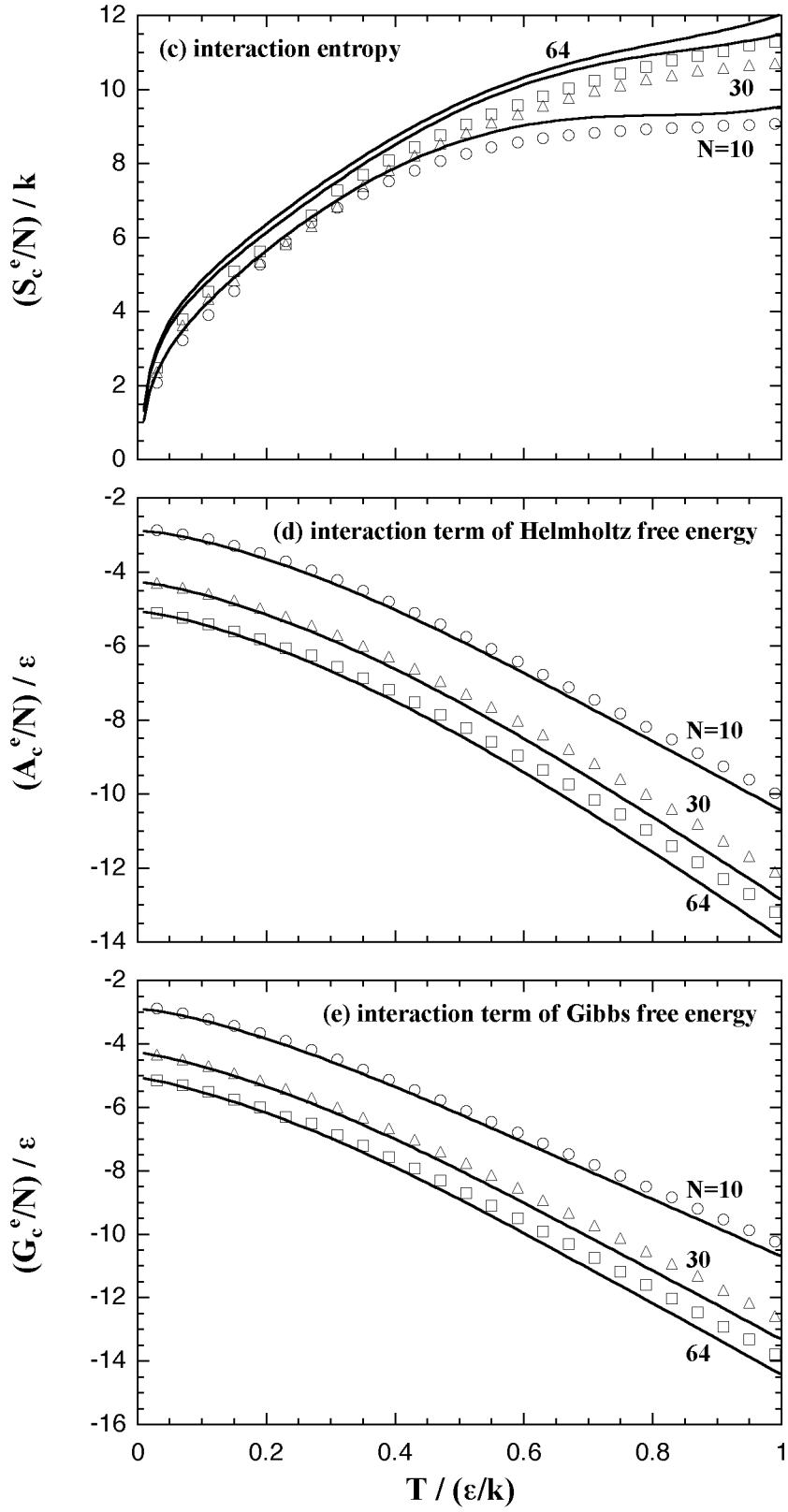

Fig. 5.9. The thermodynamic properties of the cluster phase that is derived from U_c^e and $P_c^e V$ with eqs. 2.5, 2.7, 2.3, and 2.10; (c) the interaction entropy, (d) the interaction term of the Helmholtz free energy, and (e) the interaction term of the Gibbs free energy.

5.2. Equation of State of the Nucleation Free Energy

The Helmholtz free energy of the nucleation ΔA on (N,T,V) domain is obtained by eq. 2.9. In Fig. 5.10, we compare the ΔA from the EOS and the results of the MC simulations. Figure 5.11 shows the values of the critical nucleus, the size N_A* and the nucleation energy ΔA*, that is obtained from the maximum of the nucleation energy curve like Fig. 5.10. On the other hand, as we mentioned above, the Gibbs free energy of the nucleation should be obtained under constant pressure and the ideal gas term should be included in the process of obtaining ΔG, like eqs. 2.11 and 2.12. We obtained the ΔG on (N,T,P) domain with the following procedure.

Thus far, the interaction terms of thermodynamic properties were only treated and the ideal gas terms were not considered in the purpose of the ΔA estimation. In the following, to make a relationship between the simulation results and the ideal gas, we assumed the thermodynamic properties of the monomer phase resemble those of the ideal gas. An interaction term of the Helmholtz free energy of the monomer phase can be obtained from the density integration of the compressibility factor at each number of particles as ${}_ZA_m^e$.[14]

$$\frac{\beta {}_ZA_m^e}{N} = \int_0^\rho \left(\frac{\beta P}{\rho} - 1 \right) \frac{1}{\rho} d\rho, \quad \beta = \frac{1}{kT}. \tag{5.12}$$

This is rearranged by the relation of

$$\frac{\beta P}{\rho} - 1 = \frac{\beta P_m^e}{\rho}, \tag{5.13}$$

and by the approximated function for the $P_m{}^eV$ of eq. 5.9, as

$$\frac{{}_ZA_m^e(N,V_m)}{N} = \frac{N}{V_m} \sum_{i=0}^{2} c_i N^{-i} = \frac{P_m^e V_m(N,V_m)}{N}. \tag{5.14}$$

This reestimtes the interaction term of Gibbs free energy of the monomer phase $G_m{}^e(N,T,V_m)$. On the other hand, the interaction term of Gibbs free energy of the cluster phase, $G_c{}^e(N,T,V_c)$, is obtained as

$$G_c^e(N,V_c,T) = U_c^e(N,T) - TS_c^e(N,V_c,T) + P_c^e V_c(N,T), \tag{5.15}$$

$$\begin{aligned} S_c^e(N,V_c,T) &= {}_ZS_m^e(N,V_c,T) + {}_{\mathrm{EOS}}\Delta S^e(N,V_c,T) \\ &= \frac{{}_{EOS}U_m^e(N,V_c) - {}_ZA_m^e(N,V_c)}{T} + \left\{ {}_{EOS}S_c^e(N,T) - {}_{EOS}S_m^e(N,V_c) \right\}. \end{aligned} \tag{5.16}$$

Here, we obtain the interaction entropy of the cluster phase $S_c{}^e(N,T,V_c)$ as sum of the

interaction entropy of the monomer phase and the interaction term of the entropy change between the cluster phase and the monomer phase: the former ${}_Z S_m^e$ is estimated from the compressibility factor in eq. 5.14, and the latter ${}_{\mathrm{EOS}}\Delta S^e$ is estimated from the approximated functions fo eqs. 5.10, 2.7, and 5.8. The ideal gas term of the Gibbs free energy G^{id} is defined by the statistical thermodynamics as:

$$\begin{aligned} G^{id} &= U^{id} + P^{id}V - TS^{id}, \\ U^{id} &= \frac{3}{2}NkT, \quad P^{id}V = NkT, \quad S^{id} = \frac{U^{id}}{T} + Nk\ln q - k\ln N!, \\ q &= \frac{V}{\Lambda^3}, \quad \Lambda = \frac{h}{\sqrt{2\pi mkT}}. \end{aligned} \tag{5.17}$$

Here, the symbols q, Λ, h, and m indicate the molecular partition function, the thermal wavelength, the Planck's constant, and mass of the particle. We obtained the ideal gas term of entropy with the LJ parameters and the mass of argon molecule, as ε/k = 119.8 K, σ = 0.340 nm, and m = 6.634×10^{-26} kg. Volumes of the cluster phase and the monomer phase, V_c and V_m, that present the identical pressure P, are obtained from eqs. 5.9 and 5.11 as:

$$\begin{aligned} P &= \frac{f_m}{(V_m/N)^2} + \frac{kT}{(V_m/N)} = \frac{f_c + kT}{(V_c/N)}, \\ f_m &= \sum_{i=0}^{2} c_i N^{-i}, \qquad f_c = \sum_{p=-3}^{0}\sum_{q=0}^{4} b_{pq} N^p T^q. \end{aligned} \tag{5.18}$$

The V_m/N and V_c/N at some pressures, 0.0127, 0.00679, and 0.00270 ε/σ^3, are plotted in Fig. 5.12. In the case of P = 0.0679 ε/σ^3, the V_m/N is roughly constant at 90 σ^3, while the V_c/N changes from 90.6 σ^3 at N = 2 to 10.4 σ^3 at N = 80. However, at a low temperature, it is lower than about 0.4 ε/k in the case of P = 0.00679 ε/σ^3, the V_m/N values are not available; V_m/N is obtained from the eq. 5.18 by the quadratic formula,

$$\frac{V_m}{N} = \frac{-2f_m}{kT \pm \sqrt{(kT)^2 + 4f_m P}}, \tag{5.19}$$

yet the square root term, $(kT)^2 + 4f_mP$, becomes negative at such low temperatures.

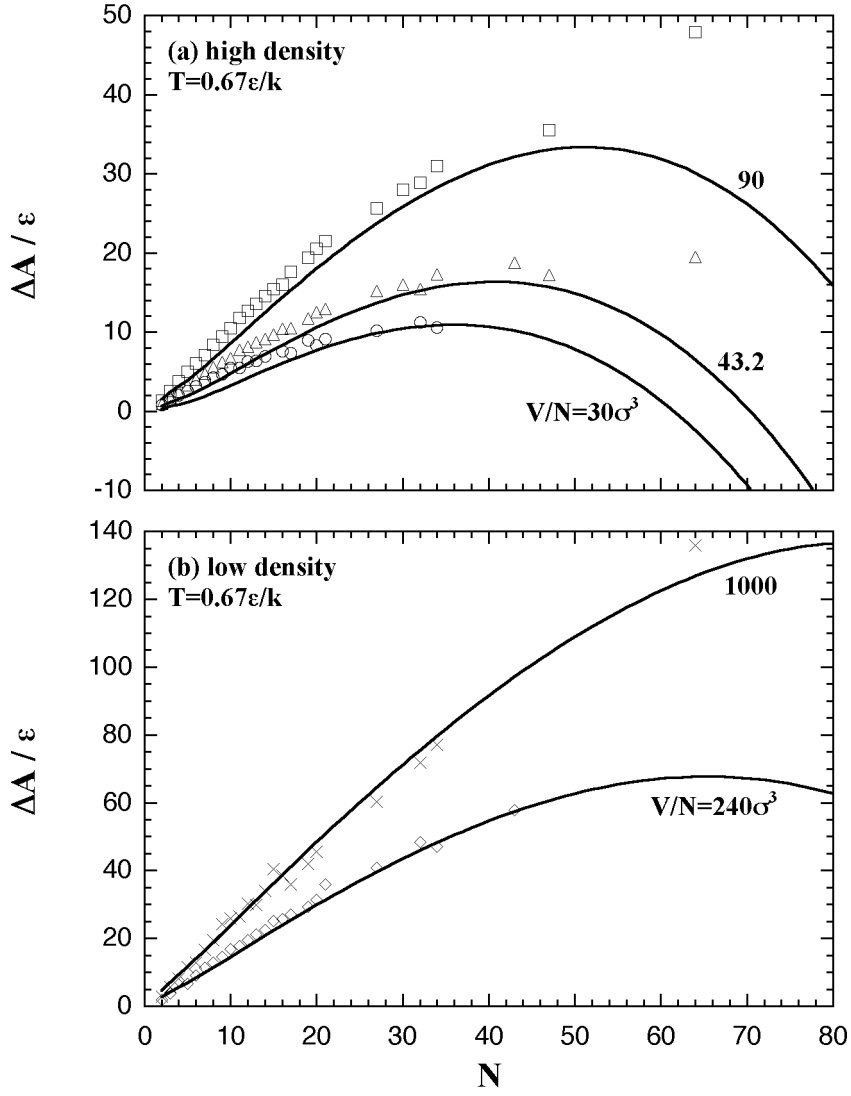

Fig. 5.10. Helmholtz free energy of the homogeneous nucleation on (*N*,*T*,*V*) domain at T = 0.67 ε/k. The curves at high-density region, V/N = 30, 43.2, and 90 σ^3, are plotted in the figure (a), while low-density in the figure (b). Circles, triangles, squares, diamonds, and crosses are the MC results and the curves are the EOS.

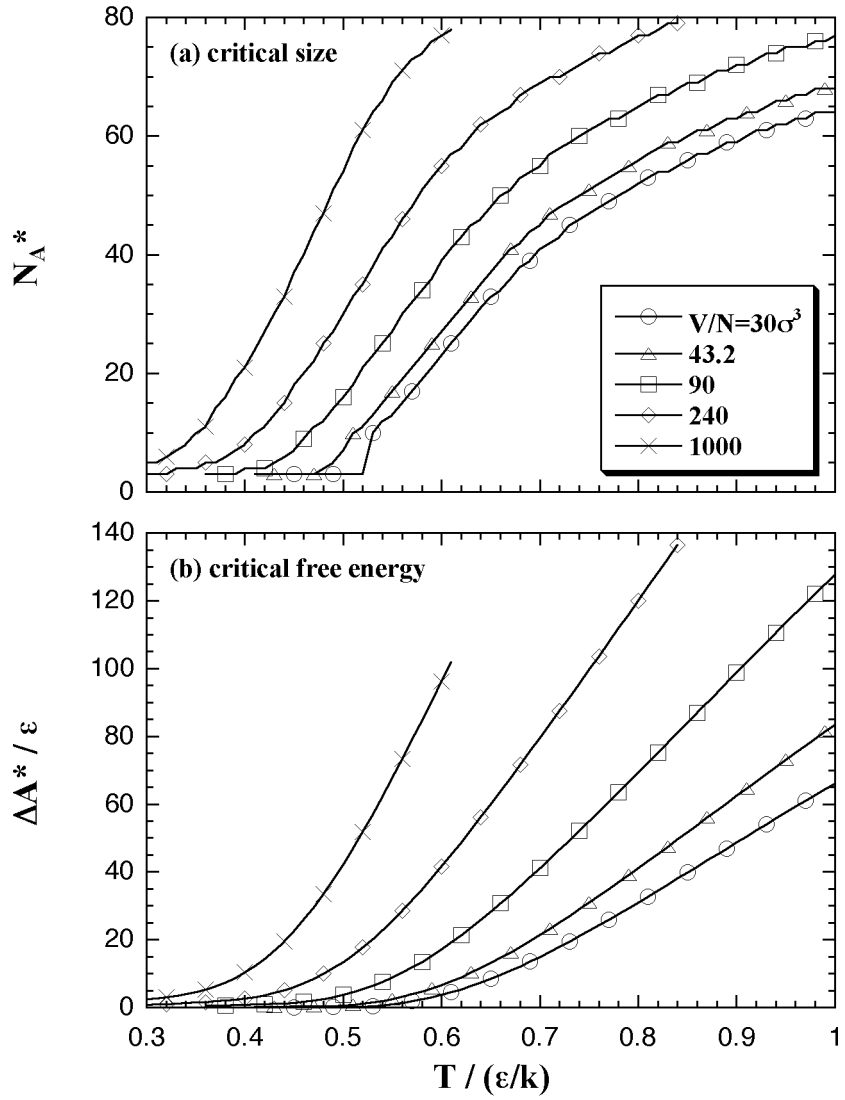

Fig. 5.11. The values of the critical nucleus on (*N*,*T*,*V*) domain: (a) the size N_A* and (b) the Helmholtz free energy Δ*A**.

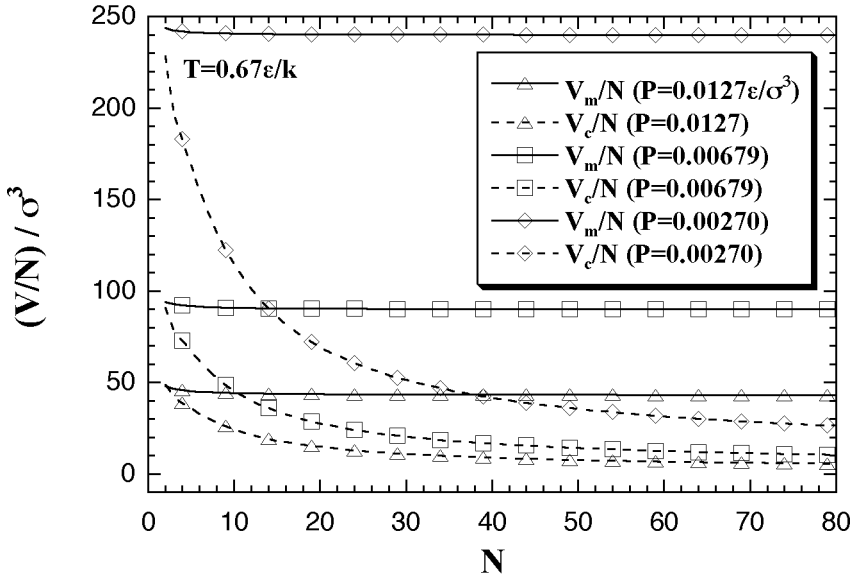

Fig. 5.12. Volumes per particle of the monomer phase and the cluster phase at T = 0.67 ε/k; that are obtained from eq. 5.18. The pressure in LJ reduced units corresponds as 1.0 ε/σ^3 = 41.9 MPa in the case of argon.

The above equations yield the Gibbs free energy of the nucleation on (N,T,P) domain with eq. 2.12. Figure 5.13 shows the $\Delta G(N,T,P)$, and Table 5 shows the components of the $\Delta G(N,T,P)$ concretely. In the high-density (high-pressure) region, Fig. 5.13 (a), the ΔG curves are somewhat overestimated; the value seems to have risen excessively at the large-N region. On the other hand, the curves of the low-density (low-pressure) region, Fig. 5.13 (b), are lower than the curves of the ΔA on corresponding volumes per particle, like Fig. 5.10. This can be explained as the following behavior of the components of ΔG and ΔA:

$$\begin{aligned}\Delta G(N,T,P) &= \Delta H_G(N,T,P) - T\Delta S_G(N,T,P) \\ &= \Delta U_G(N,T,P) + P\Delta V_G(N,T,P) - T\Delta S_G(N,T,P),\end{aligned} \tag{5.20}$$

$$\Delta A(N,T,V) = \Delta U_A(N,T,V) - T\Delta S_A(N,T,V). \tag{5.21}$$

First, we compare the internal energy term of the Gibbs free energy of the nucleation $\Delta U_G(N,T,P)$ and the one of the Helmholtz free energy $\Delta U_A(N,T,V_m)$ as:

$$\Delta U_G(N,T,P) = \left\{U_c^{id}(N,T) - U_m^{id}(N,T)\right\} + \left\{U_c^{e}(N,T) - U_m^{e}(N,V_m)\right\}, \tag{5.22}$$

$$\Delta U_A(N,T,V_m) = U_c^{e}(N,T) - U_m^{e}(N,V_m), \tag{5.23}$$

where the volume V_m gives the constant pressure P. The ideal gas term and the approximated function for the cluster phase have no dependence on the volume per particle as seen in eqs. 5.17 and 5.10. Therefore, the internal energy terms ΔU_G and ΔU_A are identical, irrespective of the volume per particle of the cluster phase. Secondly, the entropy terms, $\Delta S_G(N,T,P)$ and $\Delta S_A(N,T,V_m)$, are related in detail as:

$$\begin{aligned}\Delta S_G(N,T,P) &= \left\{S_c^e(N,T,V_c) - S_m^e(N,T,V_m)\right\} + \left\{S_c^{id}(N,T,V_c) - S_m^{id}(N,T,V_m)\right\}, \\ S_c^e(N,T,V_c) &= \frac{{}_{EOS}U_m^e(N,V_c) - {}_Z A_m^e(N,V_c)}{T} + \left\{{}_{EOS}S_c^e(N,T) - {}_{EOS}S_m^e(N,V_c)\right\}, \\ S_m^e(N,T,V_m) &= \frac{{}_{EOS}U_m^e(N,V_m) - {}_Z A_m^e(N,V_m)}{T}, \\ S_c^{id}(N,T,V_c) - S_m^{id}(N,T,V_m) &= Nk\left(\ln\frac{V_c}{\Lambda^3} - \ln\frac{V_m}{\Lambda^3}\right) = Nk\ln\frac{V_c}{V_m},\end{aligned} \tag{5.24}$$

$$\Delta S_A(N,T,V_m) = {}_{EOS}S_c^e(N,T) - {}_{EOS}S_m^e(N,V_m). \tag{5.25}$$

The expressions can be rearranged by eqs. 5.7, 5.8, and 5.14,

$$\begin{aligned}T\Delta S_G(N,T,P) &= N\left\{\sum a_i N^{-i} - \sum c_i N^{-i}\right\}\left(\frac{N}{V_c} - \frac{N}{V_m}\right) \\ &\quad + T_{EOS}S_c^e(N,T) - NT\left(\sum b_i N^{-i} + k\ln\frac{V_c}{N}\right) + NkT\ln\frac{V_c}{V_m},\end{aligned} \tag{5.26}$$

$$T\Delta S_A(N,T,V_m) = T_{EOS}S_c^e(N,T) - NT\left\{\sum b_i N^{-i} + k\ln\frac{V_m}{N}\right\}. \tag{5.27}$$

Their difference is

$$T\Delta S_G(N,T,P) - T\Delta S_A(N,T,V_m) = N\left\{\sum a_i N^{-i} - \sum c_i N^{-i}\right\}\left\{\frac{N}{V_c} - \frac{N}{V_m}\right\}, \tag{5.28}$$

this explains the contribution of the entropy term toward the difference between $\Delta G(N,T,P)$ and $\Delta A(N,T,V_m)$. The density term of eq. 5.28, $N/V_c - N/V_m$, is nearly in proportion to the pressure, i.e., becomes larger in the smaller V_m/N system as in Fig. 5.14. In the case of high-pressure and small-V_m/N system, the volume per particle of the cluster phase becomes fairly smaller: $V_c/N \sim 4.3\ \sigma^3$ at $P = 0.0165\ \varepsilon/\sigma^3$, $N = 80$, and $T = 0.67\ \varepsilon/k$. We assumed that the thermodynamic properties of the cluster phase, U_c^e, S_c^e, and $P_c^e V_c$, do not depend on the density such as eqs. 5.10 and 5.11, that is based on the MC results of $V_c/N = 30$ up to $1000\ \sigma^3$ as in Figs. 5.5. and 5.6. However, it is not guaranteed that the thermodynamic properties of the cluster phase are constant against the density in the high-density region as $V_c/N < 30\ \sigma^3$, and the EOS extrapolates the V_c/N in the high-density region. Possibly, in the high-density region, the density dependence that we neglected becomes remarkable; therefore the EOS would contain overestimate the ΔG. On contrary, in low-pressure/low-density region, the EOS of ΔG is in consistent with the one of ΔA because the extrapolation is not remarkable. Figure 5.15 shows the behavior of the components of the nucleation energy: $\Delta U_G(N,T,P)$, $P\Delta V_G(N,T,P)$, and $T\Delta S_G(N,T,P)$ of the ΔG, besides $\Delta U_A(N,T,V)$ and $T\Delta S_A(N,T,V)$ of ΔA. The effect of the extrapolation in high-pressure/high-density region as the figure (a) is much larger than the one in low-pressure/low-density as (b); the deviation of the $T\Delta S_G$ term raises the ΔG as in figure (a).

Here, we consider the reason what the ΔG curve obtains a maximum against the number of particles. The ΔG can be divided into the enthalpy term and the entropy term as in eq. 5.20, while into the ideal gas term and the interaction term as

$$\Delta G = \Delta G^{id} + \Delta G^e. \tag{5.29}$$

Such components are plotted in Fig. 5.16. In the figure, the ideal gas term is plotted as $-\Delta G^{id}$, then eq. 5.29 can be interpreted as $\Delta G = \Delta G^e - (-\Delta G^{id})$. In the small-$N$ region, the enthalpy term or the interaction term (solid curves) is higher than the entropy term or the ideal gas term (broken curves), and inclination of the former is less than that of the latter. Therefore, the ΔG has a positive value and increases against the number of particles for a

while. However, after all, the enthalpy term or the interaction term overtakes the entropy term or the ideal gas term due to increase of the inclination of the formers. Accordingly, the ΔG has a maximum as in Fig. 5.13. The values of the critical nucleus given by the maximum, the size of N_G* and the free energy of ΔG*, are plotted in Fig. 5.17 as a function of temperature.

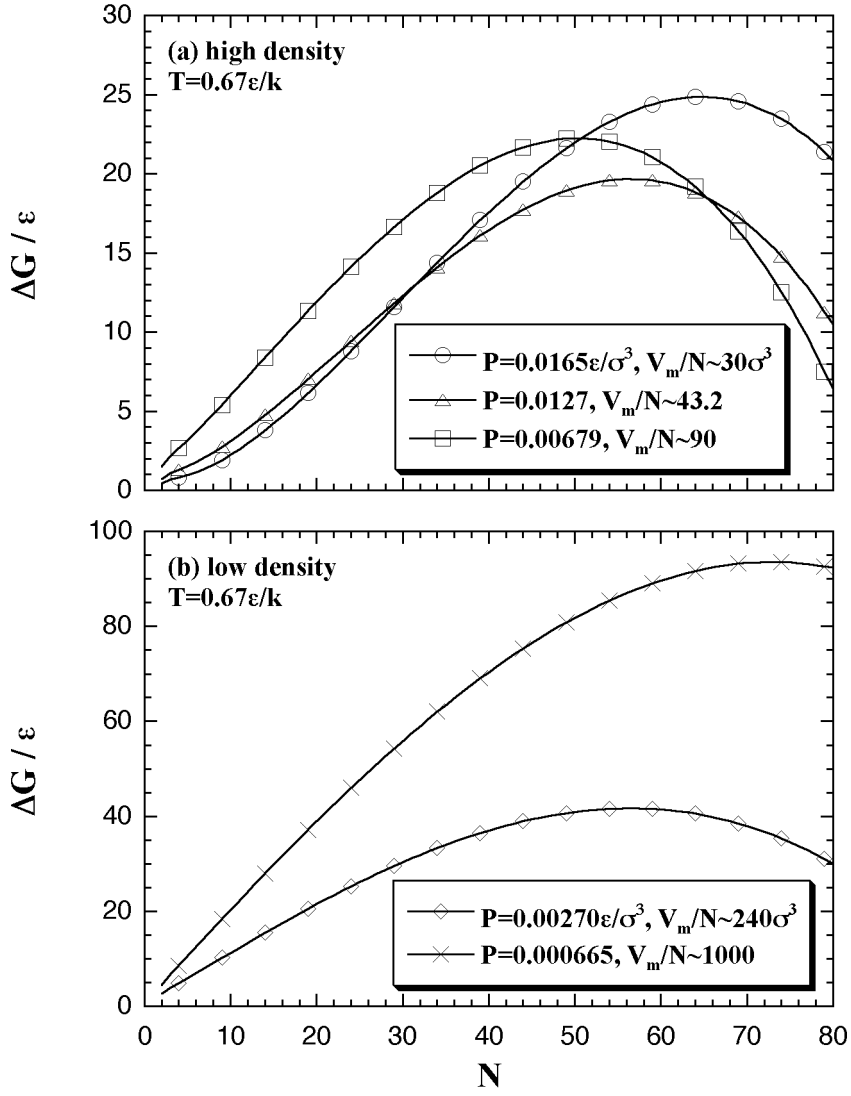

Fig. 5.13. Gibbs free energy of the homogeneous nucleation on (*N*,*T*,*P*) domain. The contribution of the ideal gas term is taken into consideration in the ΔG estimation. The volumes per particle of the monomer phase are mostly close to the figured values at which maxima.

Table 5. Examples of the concrete values that construct the nucleation energy at P = 0.0127, 0.00679, and 0.00270 ε/σ^3. The number of particles and the temperature are constant as N = 32 and T = 0.67 ε/k.

P / (ε/σ^3)		(V/N) / σ^3		U / ε	S / k	PV / ε	G / ε
1.27E−2	cluster	4.34E+1	ideal	4.12E+1	5.09E+2	2.75E+1	−2.73E+2
			interaction	−1.05E+2	−1.45E+2	−2.29E+1	−3.07E+1
	monomer	1.04E+1	ideal	4.12E+1	5.80E+2	2.75E+1	−3.20E+2
			interaction	−4.62E+0	−3.33E+0	−2.39E+0	−4.77E+0
	delta	3.29E+1	ideal	0	−7.02E+1	0	4.70E+1
			interaction	−1.00E+2	−1.41E+2	−2.06E+1	−2.60E+1
6.79E−3	cluster	9.01E+1	ideal	4.72E+1	5.80E+2	3.15E+1	−3.10E+2
			interaction	−1.27E+2	−1.70E+2	−2.68E+1	−4.03E+1
	monomer	1.95E+1	ideal	4.72E+1	6.65E+2	3.15E+1	−3.67E+2
			interaction	−5.32E+0	−3.84E+0	−2.75E+0	−5.49E+0
	delta	7.07E+1	ideal	0	−8.50E+1	0	5.69E+1
			interaction	−1.22E+2	−1.66E+2	−2.40E+1	−3.48E+1
2.70E−3	cluster	2.40E+2	ideal	3.22E+1	4.32E+2	2.14E+1	−2.36E+2
			interaction	−7.27E+1	−1.29E+2	−1.72E+1	−3.58E+0
	monomer	4.90E+1	ideal	3.22E+1	4.83E+2	2.14E+1	−2.70E+2
			interaction	−1.34E+0	−9.66E−1	−6.94E−1	−1.39E+0
	delta	1.91E+2	ideal	0	−5.09E+1	0	3.41E+1
			interaction	−7.14E+1	−1.28E+2	−1.65E+1	−2.19E+0

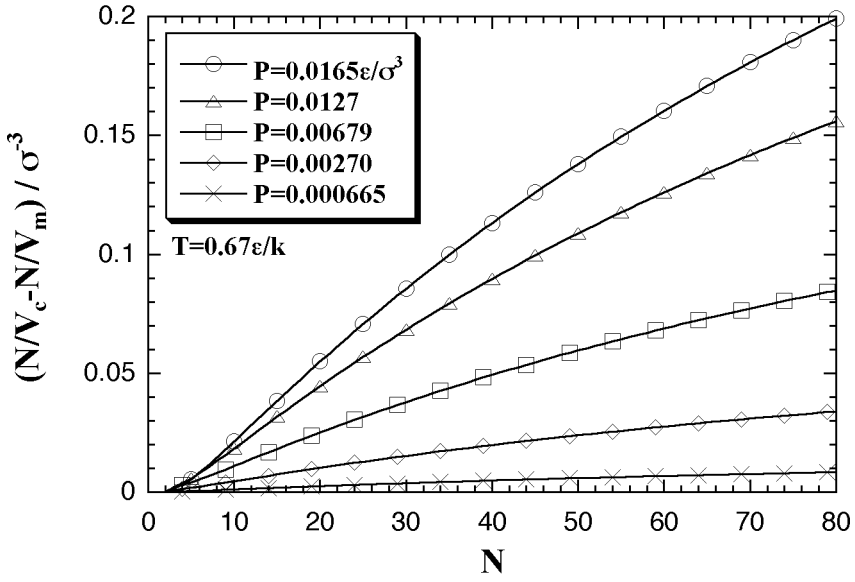

Fig. 5.14. Pressure dependence of the density term of the contribution of the entropy term toward the difference between $\Delta G(N,T,P)$ and $\Delta A(N,T,V_m)$; shown in eq. 5.28. When the pressure becomes lower (V_m/N larger), the density term and eq. 5.28 becomes smaller.

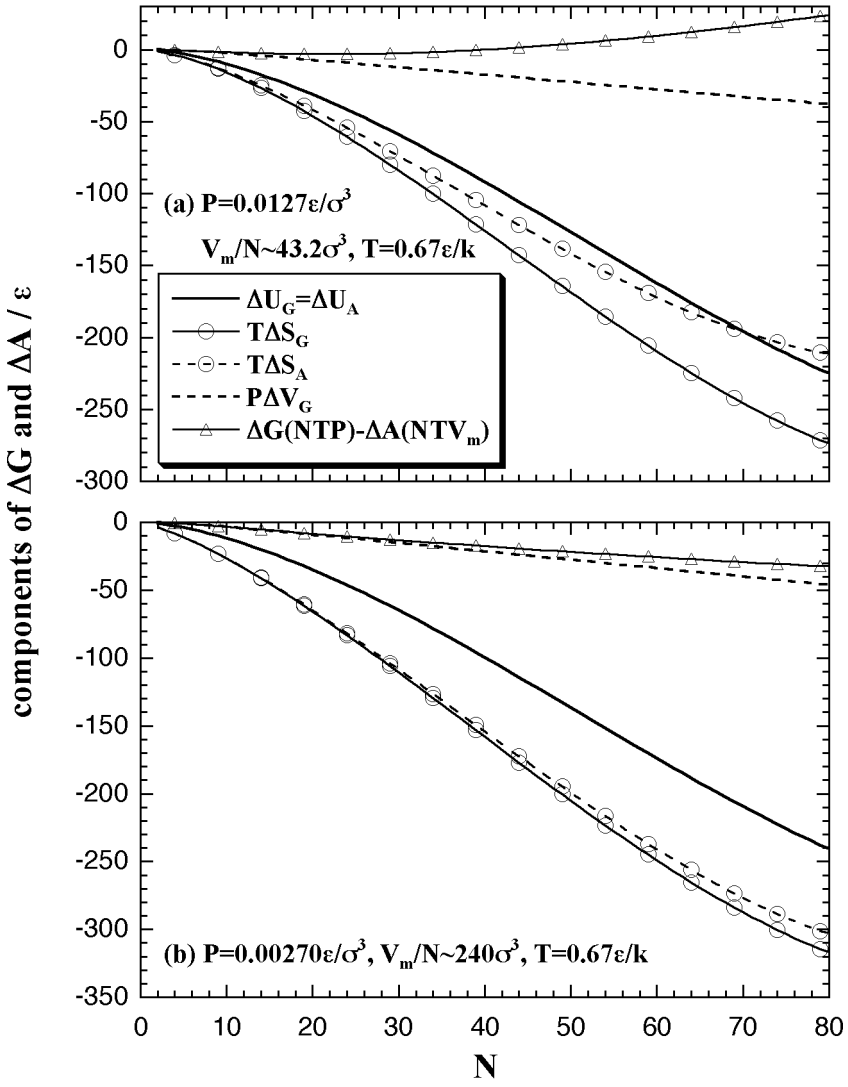

Fig. 5.15. Components of ΔG and ΔA versus N plots. In the high-pressure system (a), the difference $T\Delta S_G - T\Delta S_A$ becomes remarkable with the increase of N, it cancels the negative contribution of the $P\Delta V_G$ and raises the ΔG. On the other hand, the low-pressure (b), the difference between the entropy terms becomes smaller, therefore the difference $\Delta G - \Delta A$ is almost occupied by the $P\Delta V_G$ contribution and the ΔG becomes lower than the ΔA.

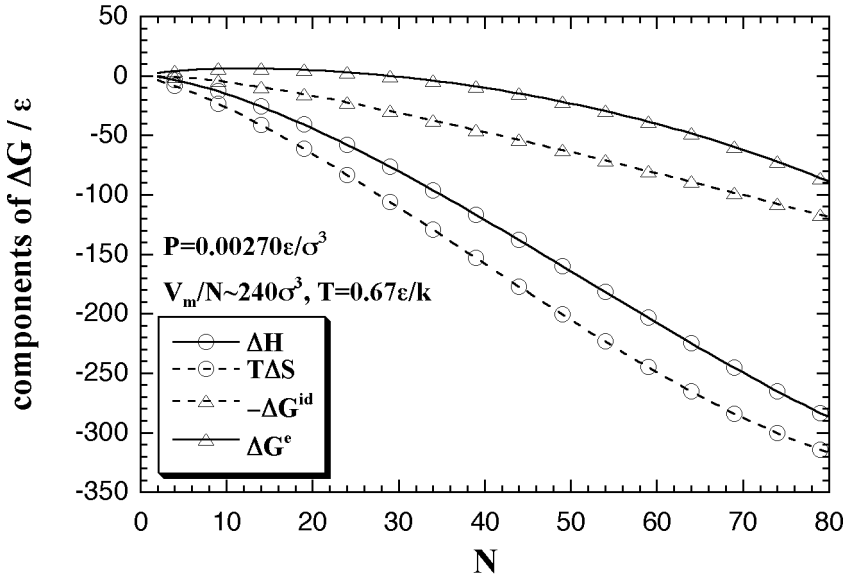

Fig. 5.16. The components of ΔG; the entropy term ΔH and the entropy term $T\Delta S$, while the ideal gas term ΔG^{id} and the interaction term ΔG^{e} at $P = 0.00270\ \varepsilon/\sigma^3$ and $T = 0.67\ \varepsilon/k$. Care should be taken that the ideal gas term is plotted as $-\Delta G^{id}$.

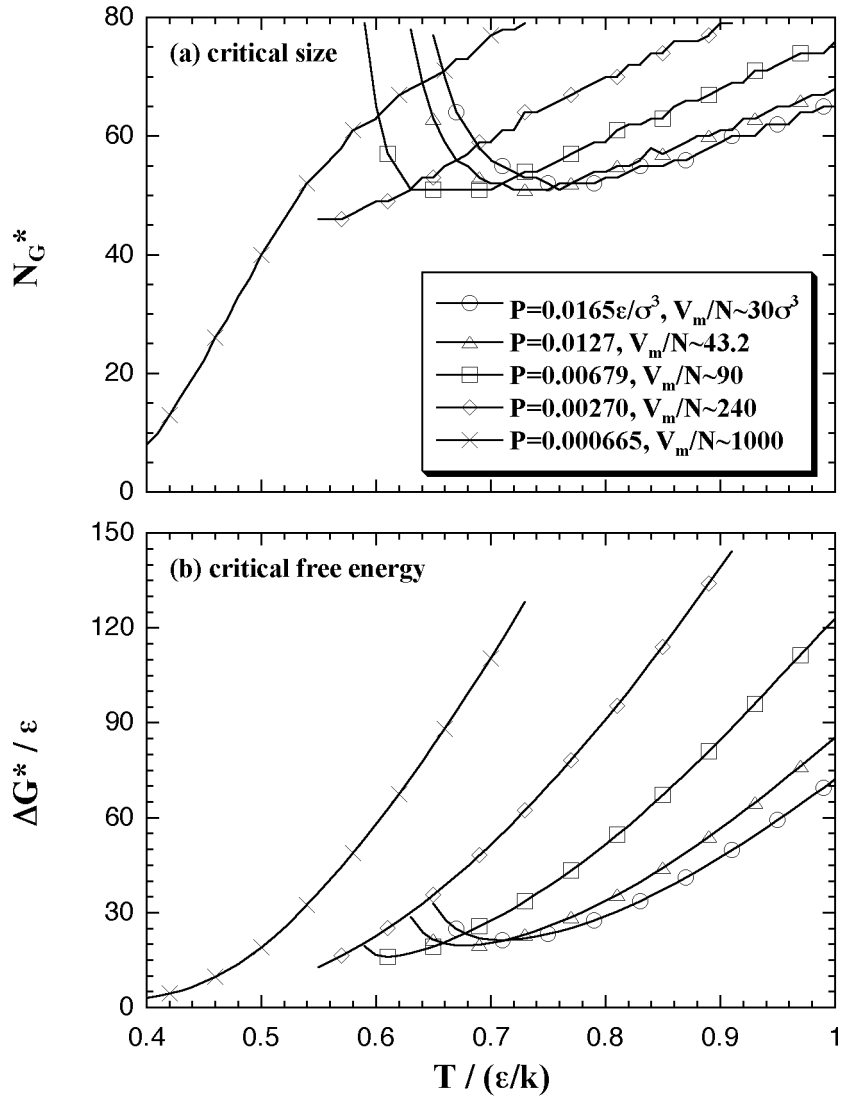

Fig. 5.17. The values of the critical nucleus in (*N*,*T*,*P*) domain: (a) the size N_G* and (b) the Gibbs free energy Δ*G**. As we stated in the text, the both N_G* and Δ*G** are overestimated at the high-pressure system.

5.3. Comparison with the Classical Nucleation Theory and Other Simulations

According to the classical nucleation theory as stated in section 1.2.2, the free energy of nucleation is expressed as a function of the number of particles:

$$\Delta G = 4\pi\gamma\left(\frac{3N}{4\pi\rho_c}\right)^{2/3} - NkT\ln S. \tag{1.14}$$

Here, the supersaturation ratio $S = (P/P_e)$ is also regarded as (ρ/ρ_e); ρ and ρ_e are densities of the supersaturated vapor and equilibrated vapor phases, besides $\gamma = 1.03\ \varepsilon/\sigma^2$, $\rho_c = 0.82\ \sigma^{-3}$, and $\rho_e = 0.00161\ \sigma^{-3}$ at $T = 0.67\ \varepsilon/k$. We compared the EOS and the classical theory in Fig. 5.18. The classical theory underestimates the size of the critical nucleus N_G*, and overestimates the critical free energy ΔG*, these have been reported in computational and experimental results.[17,18] Though the EOS also overestimates in both N_G* and ΔG*, the values seem to be consistent with the inclination of the classical theory.

The size and the free energy of the critical nucleus are obtained as eqs. 1.15 and 1.13:

$$N_G^* = \frac{32\pi\gamma^3}{3\rho_c^2(kT\ln S)^3}, \tag{1.15}$$

$$\Delta G^* = \frac{16\pi\gamma^3}{3(\rho_c kT\ln S)^2}. \tag{1.13}$$

Figure 5.19 shows the comparison between the results of the EOS and the other simulations. Oh and Zeng estimated the N_G* and ΔG* of the LJ system by MC simulations of the nucleation in a large system in which they set an upper limit of the size of cluster.[5] Yasuoka and Matsumoto performed MD simulations for the nucleation of LJ system, and also obtained the N_G* and ΔG*.[3] As we stated in previous section, since the EOS overestimates the ΔG in high-density region by the effect of the extrapolation of the V_c/N, the reliability of the EOS is scanty in the high-density region. However, it can be expected that the EOS will give a suitable prediction qualitatively except for the region that the N* and the ΔG* rise against density increase, ca. $V_m/N < 100\ \sigma^3$.

In the classical theory, the ΔG gives a maximum against the cluster size due to competition between the surface and the bulk contributions. The classical theory is a prediction from the macroscopic phenomenology. On the other hand, in the EOS from the microscopic MC simulations, the maximum is obtained due to competition between the

enthalpy and the entropy terms or the interaction and the ideal gas terms, as stated above. The model daringly simplified the N-particle nucleation as monomer-cluster transition in an N-particle system. Still the model gave the maximum values of ΔG (and ΔA) near to the prediction of the classical theory, and was consistent qualitatively with the classical theory. The agreement suggests that, though many examinations are required, the model is available to predict the nucleation energy.

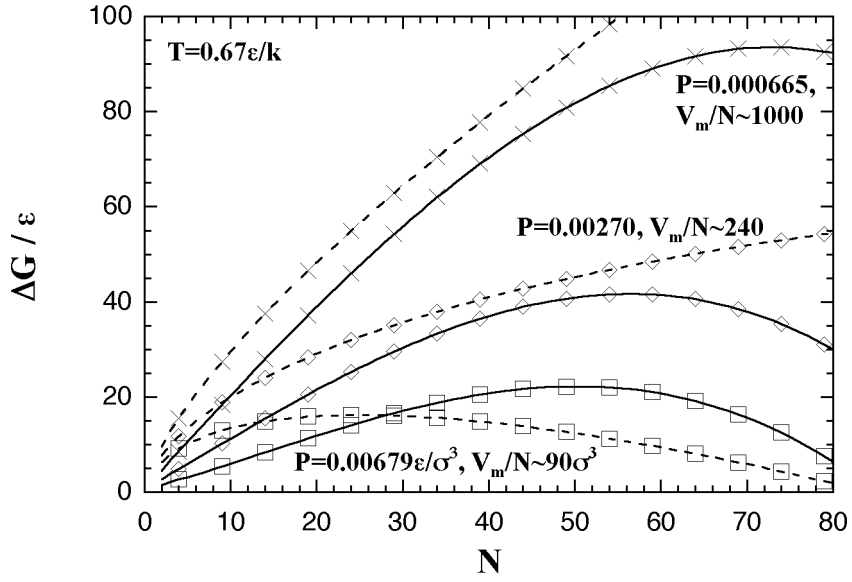

Fig. 5.18. Comparison between the EOS and the classical nucleation theory at T = 0.67 ε/k. The former is plotted as solid curves, and the latter broken curves.

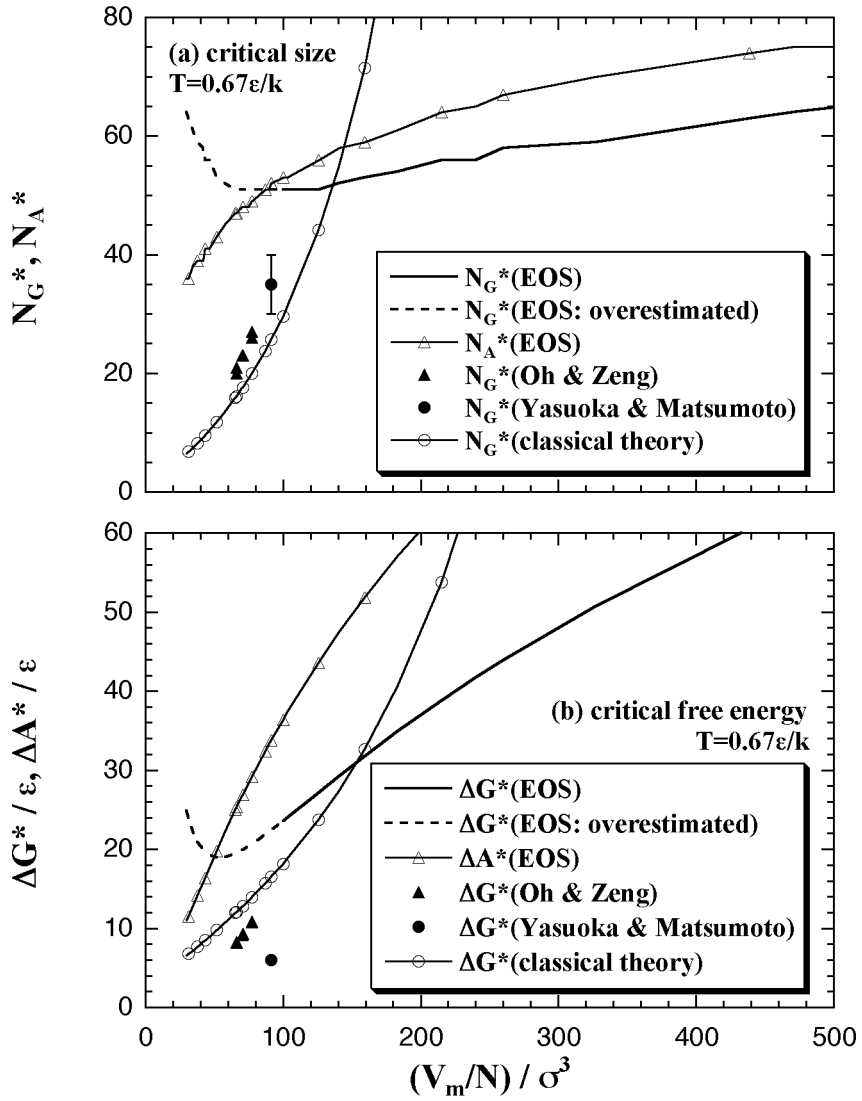

Fig. 5.19. Comparison between the EOS and other simulations in the values of the critical nucleus at $T = 0.67\ \varepsilon/k$. The prediction of the classical theory is also plotted. In high-density region, ca. $V_m/N < 100\ \sigma^3$, the EOS of the Gibbs free energy somewhat overestimates in which critical values; the region is plotted as the broken curves.

Chapter 6: CONCLUSION

In this thesis, we estimated the free energy of the homogeneous nucleation in the supersaturated Lennard-Jones vapor phase by using the Monte Carlo simulations. The MC simulations are performed on the various numbers of particles and volumes per particle at 128 states. From the MC results, we assumed an equation of state for the free energy of the homogeneous nucleation as a function of the number of particles, the temperature, and the volume per particle. The EOS clarified the characteristics of the nucleation energy against these variables. The results obtained in this work are concluded as follows.

First, we focused a specific N-particle nucleation, and daringly simplified the nucleation as the phase transition between the two extremes of the N-particle system, i.e., from the monomer phase to the cluster phase. In the former, the N particles scatter as the supersaturated vapor phase, while in the latter, on contrary, the N particles connect together as a unity cluster. If the free energies of the monomer phase and the cluster phase in the N-particle system are estimated independently, which difference obtains the N-particle nucleation free energy. In the simulations of the cluster phase, we restricted the system configuration to keep a unity cluster in the whole range of the simulated temperature by the Stillinger's cluster criterion. In which the all particles of the system should be connected together, and the connection is decided by a threshold value of the interparticle distance. We obtained the interaction part of the Helmholtz free energy under constant volume per particle as sum of the interaction energy and the interaction entropy term. The interaction entropy was estimated by the thermodynamic integration from the interaction energy, as the relative value from the low temperature.

Secondly, the Helmholtz free energy gave a maximum (the critical nucleus) against the number of cluster particles under representative temperature (near the triple point temperature of the LJ fluid) and volume per particle. That has been studied widely by the small- and large-scale simulations, in which the critical nucleus were similarly obtained.

Thirdly, we designed the equation of state for the Helmholtz free energy of the

homogeneous nucleation by the results of MC simulations at the 128 states. From the EOS, we suggested a reason what the nucleation energy has a maximum against the number of particles; that is caused by competition between the internal energy term and the entropy term of the nucleation energy.

Lastly, we suggested a method that rearranges the EOS for estimating Gibbs free energy of the homogeneous nucleation as a function of the number of particles, the temperature, and the pressure. The EOS gave the maximum and behaved similarly to the one of the Helmholtz free energy in which low-pressure/low-density region. Though the EOS still has unsatisfied problems as the overestimation of the nucleation energy in which high-pressure/high-density region, it is variable as a technique for estimating the EOS of the Gibbs free energy of the homogeneous nucleation from the microscopic MC simulations with the simplified model.

REFERENCES

† D. Kashchiev, "Nucleation: Basic Theory with Applications," Butterworth-Heinemann, Oxford (2000).

† R. J. Sadus, "Molecular Simulation of Fluids: Theory, Algorithms and Object-Orientation," Elsevier, Amsterdam (1999).

1 M. Volmer and A. Weber, *Z. Phys. Chem.*, **119**, 277 (1926).

2 K. Yasuoka, Ph.D. Thesis, Nagoya University (1997).

3 K. Yasuoka and M. Matsumoto, *J. Chem. Phys.*, **109**, 8451 (1998).

4 K. Yasuoka and M. Matsumoto, *J. Chem. Phys.*, **109**, 8463 (1998).

5 K. J. Oh and X. C. Zeng, *J. Chem. Phys.*, **110**, 4471 (1999).

6 K. J. Oh and X. C. Zeng, *J. Chem. Phys.*, **112**, 294 (2000).

7 P. R. ten Wolde and D. Frenkel, *J. Chem. Phys.*, **109**, 9901 (1998).

8 I. Kusaka and D. W. Oxtoby, *J. Chem. Phys.*, **110**, 5249 (1999).

9 J. M. Haile, "Molecular Dynamics Simulation: Elementary Methods," Wiley Interscience, New York (1992).

10 N. Bernardes, *Phys. Rev.*, **112**, 1534(1958).

11 J. J. Nicolas, G. E. Gubbins, W. B. Streett, and D. J. Tildesley, *Mol. Phys.*, **37**, 1429 (1979).

12 F. H. Stillinger, *J. Chem. Phys.*, **38**, 1486 (1963).

13 Y. Kataoka and M. Matsumoto, *Bull. Chem. Soc. Jpn.*, **70**, 1795 (1997).

14 F. H. Ree, *J. Chem. Phys.*, **73**, 5401 (1980).

15 F. F. Abraham and J. A. Barker, *J. Chem. Phys.*, **63**, 2266 (1975).

16 A. Laaksonen, V. Talanquer, and D. W. Oxtoby, *Ann. Rev. Phys. Chem.*, **46**, 489 (1995).

17 X. C. Zeng and D. W. Oxtoby, *J. Chem. Phys.*, **94**, 4472 (1991).

18 C. Hung, M. J. Krasnopolar, and J. L. Katz, *J. Chem. Phys.*, **90**, 1856 (1989).

†: referred throughout in this thesis.

[References in Japanese]

† **岡田 勲、大澤 映二編、「分子シミュレーション入門」、海文堂**(1989).
† **上田顯、「コンピュータシミュレーション」、朝倉書店**(1990).
† **片岡洋右、「分子動力学法とモンテカルロ法」、講談社サイエンティフィク**(1994).
† **川添良幸・三上益弘・大野かおる、「コンピュータ・シミュレーションによる物質科学:分子動力学法とモンテカルロ法」、共立出版**(1996).
† **小竹進、「熱流体の分子動力学」、丸善**(1998).
† P. W. Atkins、**千原秀昭・中村亘男訳、「物理化学」第 4 版上・下、東京化学同人**(1993).
I **黒田登志雄、「結晶は生きている」、サイエンス社**(1984).
II L. N. Israelachvilli、**近藤保・大島広行訳、「分子間力と表面力」、朝倉書店**(1991).
III **片岡洋右、*熱物性*、13、**74 (1999).
IV **渡辺力・名取亮・小国力監修、「**Fortran 77 **による数値計算ソフトウェア」、丸善**(1989).
V **梶本興亜編、「クラスターの化学」、培風館**(1992).
VI **菅野暁、・近藤保・茅幸二編、「新しいクラスターの化学」、講談社サイエンティフィク**(2002).

Appendix A: GIBBS-THOMSON'S FORMULA[V]

As stated in Sec. 1.2.1, the equilibrium pressure of the small-size cluster with the radius of r is expressed by the relationship with the equilibrium pressure of the bulk liquid phase by Gibbs-Thomson's formula as

$$\ln\frac{P(r)}{P_e} = \frac{2\gamma}{\rho_c kTr}. \tag{1.9}$$

In this appendix, this formula is explained in detail by comparison between the condensation/evaporation process on surface of the bulk liquid phase and the one of the cluster.

Here, we consider a spherical cluster with the radius of r. When the cluster grows in which radius to $r + dr$, the surface area of the cluster increases as

$$4\pi(r + dr)^2 - 4\pi r^2 \quad 8\pi r dr. \tag{A.1}$$

Thus, the surface excess energy of the cluster increases $8\pi r dr\gamma$ against the increase of the radius dr. From the relation between the number of the cluster molecules and the cluster radius as $N = (4/3)\pi r^3\rho_c$, change of the number of the cluster molecules against the cluster radius, dN/dr, is

$$\frac{dN}{dr} = d\left(\frac{4}{3}\pi r^3\rho_c\right)\Big/ dr = 4\pi r^2\rho_c. \tag{A.2}$$

Accordingly, the surface excess energy of the cluster increases against the increase of N particles as

$$8\pi r\gamma\frac{dr}{dN} = \frac{2\gamma}{r\rho_c}. \tag{A.3}$$

When a cluster with the radius of r equilibrates in supersaturated vapor, i.e. when the system pressure $P = P(r)$, chemical potential of the cluster $\mu_{\text{cluster}}(r)$ and the one of the vapor phase μ_{vapor} are identical:

$$\mu_{\text{cluster}}(r) = \mu_{\text{vapor}}. \tag{A.4}$$

Since the $\mu_{\text{cluster}}(r)$ indicates the free energy change per cluster molecule, it relates to the

chemical potential of the bulk liquid phase (with flat surface as $r = \infty$) as:

$$\mu_{\text{cluster}}(r) = \mu_{\text{cluster}}(\infty) + \frac{2\gamma}{r\rho_c}. \tag{A.5}$$

The difference of eqs. A.4 and A.5 is

$$\mu_{\text{vapor}} - \mu_{\text{cluster}}(\infty) = \frac{2\gamma}{r\rho_c}. \qquad [P = P(r)] \tag{A.6}$$

On the other hand, in the liquid-vapor equilibrium, i.e. $P = P_e$, chemical potentials of the both phases are identical:

$$\mu_{\text{vapor}} - \mu_{\text{cluster}}(\infty) = 0. \qquad [P = P_e] \tag{A.7}$$

The difference of eqs. A.6 and A.7 gives the relation of $P(r)$ and P_e. Now, the Gibbs free energy of the system G is expressed against the minute changes of the temperature dT and the pressure dP as

$$dG = VdP - SdT, \tag{A.8}$$

where V is the volume and S thr entropy. If the vapor phase is assumed as an ideal gas, the free energy change of the isothermal compression from P_e to $P(r)$ is

$$\Delta G = \int_{P_e}^{P(r)} VdP = NkT \int_{P_e}^{P(r)} \frac{dP}{P} = NkT \ln \frac{P(r)}{P_e}. \tag{A.9}$$

In the bulk phase, the chemical potential equals to the Gibbs free energy per molecule, then

$$\mu_{vapor}[P(r)] - \mu_{vapor}[P_e] = kT \ln \frac{P(r)}{P_e}. \tag{A.10}$$

On the other hand, in the case of the liquid phase, since the volume can be considered as almost constant against the compression:

$$\mu_{\text{cluster}}(\infty)[P(r)] - \mu_{\text{cluster}}(\infty)[P_e] \sim 0. \tag{A.11}$$

Accordingly, the relation of $P(r)$ and P_e is expressed with eqs. A.6, A.7, A.10, and A.11 as

$$kT \ln \frac{P(r)}{P_e} = \frac{2\gamma}{\rho_c r}. \tag{A.12}$$

Appendix B: STABLE STRUCTURE AND THE MAGIC NUMBER OF SMALL-SIZE CLUSTER[V,VI]

Materials form the specific crystal structures by which kind(s) of molecule: cubic lattice, tetragonal lattice, hexagonal lattice, diamond structure, etc. However, the small-size cluster has another structure because the contribution of the cluster surface is much larger than the bulk crystal. The noble gases, neon, argon, krypton, and xenon, form the face-centered cubic (fcc) lattice as the most stable structure of the bulk crystal phase at low temperature. On the other hand, in the small-size cluster of the noble gases, the intermolecular interaction is almost occupied by the dispersion force, therefore the cluster stability is ruled by the geometrical configuration of the molecules. The regular icosahedral structure with the 5-fold axis of symmetry is the most stable structure of the small-size cluster of the noble gases, and the Lennard-Jones particles.

The number of particles that realizes the icosahedral structure is $N = 13$, 55, 147, 309, and more. These sizes of clusters have exceptional stability, so the numbers are termed as the Magic Numbers. In the case of 13-particle icosahedral cluster, there is a particle at the center of mass of the icosahedron and the rest of 12 particles surround the center particle at each vertex of the icosahedron. On the other hand, in the case of a unit lattice of fcc, a particle is also surrounded by 12 particles by which nearest neighbours. Figure B.1 shows a comparison between the icosahedral structure and the corresponding fcc structure. The both configurations resemble each other, then the one side can convert easily to the other.

In the MC simulations under a fixed volume per particle (Chapter 3; explained in detail in Chapter 2), we chose a distorted cubic lattice as an initial configuration of the cluster stabilization process. However, in the simulation on various volumes per particle (Chapter 4), the initial configuration was only the fcc lattice. That is caused by a difficulty of the cluster stabilization when we chose the simple cubic lattice or body-centered cubic lattice as the initial configuration. However, as the results, all the stabilized clusters had the icosahedral structure or the resemble one; except for very smaller clusters as $N < 7$, that

form triangle, octahedron, decahedron, etc. Accordingly, the fcc (also the simple cubic and the body-centered cubic) lattices are suitable as an initial configuration of the cluster stabilization process. Figure B.2 shows the configurations at the end of the cluster stabilization process.

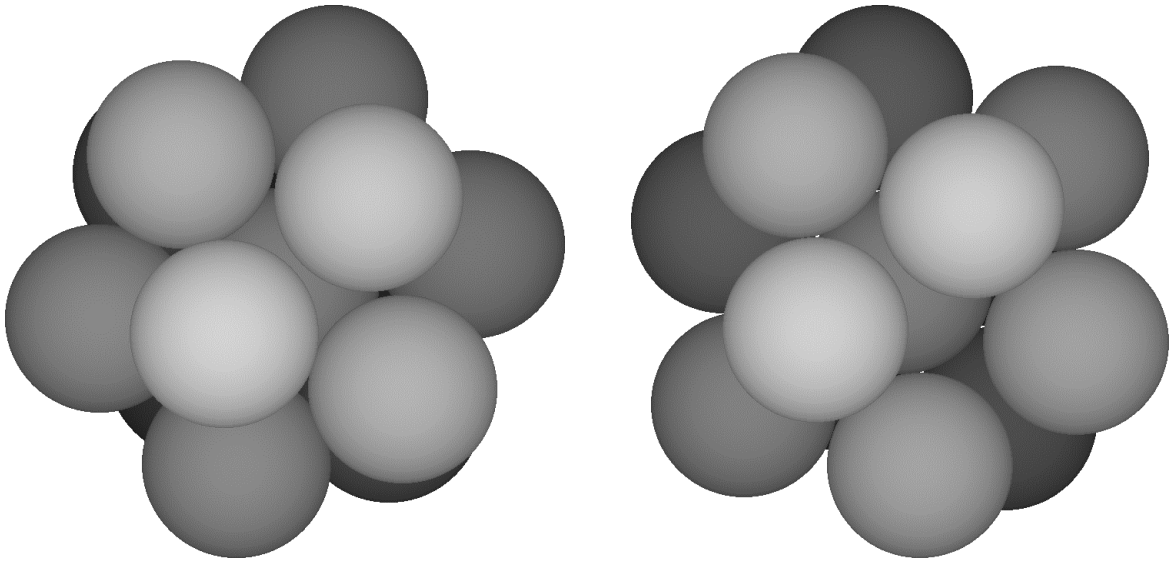

Fig. B.1. Comparison of the configurations of the icosahedron (the left figure) and the fcc (the right). The fcc lattice has the 2-, 3-, and 4-fold axes of symmetries, while the icosahedron has the 2-, 3-, and 5-fold axes of symmetries. Yet, the both structures resemble each other.

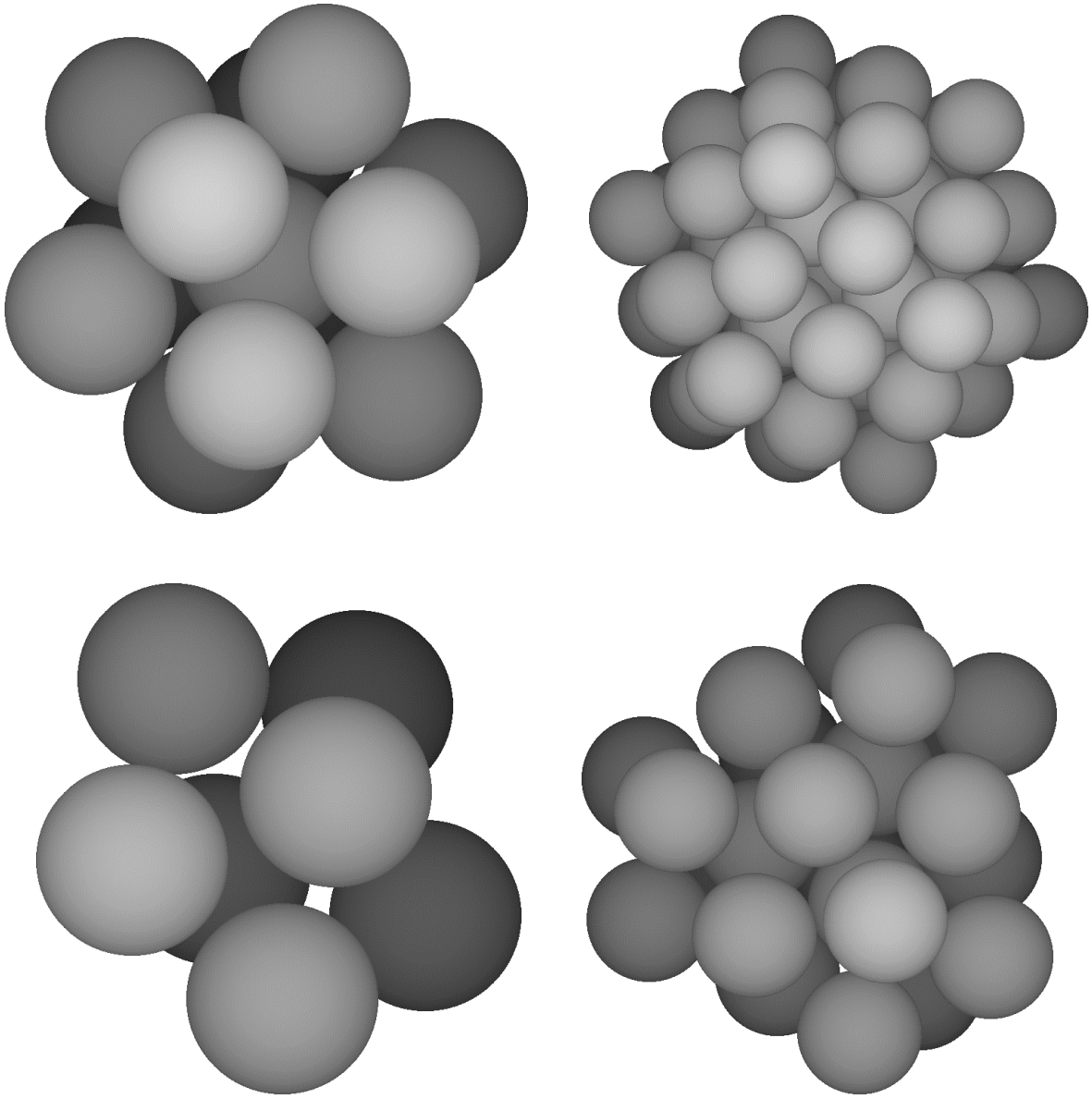

Fig. B.2. The characteristic snapshots of the stabilized clusters of the MC simulations, corresponding to Fig. 2.5. The snapshots in top are the Magic Number clusters; N = 13 and 55. The bottom left is the decahedral structure on N = 7, while the bottom right N = 23, it has also geometrical stability.